

On the Formation of Stellar Clusters: Gaussian Cloud Conditions II

Ralf S. Klessen^{1,2} and Andreas Burkert²

¹Sterrewacht Leiden, Postbus 9513, 2300-RA Leiden, The Netherlands

²Max-Planck-Institut für Astronomie, Königstuhl 17, 69117 Heidelberg, Germany

ABSTRACT

Using hydrodynamic simulations we investigate the time evolution and fragmentation of regions within molecular clouds which have lost their turbulent support leading to gravitational contraction. The initial density distributions are described by random Gaussian fluctuations with varying slopes ν of the power spectrum $P(k) \propto k^{-\nu}$, covering the range from flat ($\nu = 0$) to very steep spectra ($\nu = 3$). We consider molecular cloud volumes containing different masses relative to the average Jeans mass M_J , from $1 M_J$ to $222 M_J$. This parameter study extends the detailed analysis of systems with initially $P(k) \propto k^{-2}$ and mass $222 M_J$ presented by Klessen & Burkert (2000).

The dynamical evolution of the simulated molecular cloud regions is insensitive to the slope of the initial density fluctuation spectrum. The system evolves into a complex network of intersecting filaments and collapsing clumps leading to the formation of a compact cluster of accreting and interacting embedded protostellar cores. The cluster builds up as bound entity, but dissolves later due to collisional effects. In all simulations, the mass spectrum of collapsed cores is very broad, has approximately log-normal shape and peaks roughly at the average Jeans mass. This supports the hypothesis that the average Jeans mass is the main parameter determining the peak in the stellar spectrum, and suggests that the interplay between self-gravity on the one side and thermal and turbulent pressure on the other side is the dominant process that regulates the formation of stellar clusters.

Subject headings: hydrodynamics – ISM: clouds – ISM: kinematics and dynamics – ISM: structure – stars: formation – turbulence

1. Introduction

Understanding the processes that lead to the formation of stars is one of the fundamental challenges in astronomy. All presently known star formation takes place in turbulent

interstellar clouds of cold molecular hydrogen. The formation of molecular clouds out of the diffuse and warm atomic interstellar medium is not fully understood, and probably involves large-scale compressible turbulence, chemical phase transitions, and a combination of different instability mechanisms including gravitational, thermal, Kelvin-Helmholtz and Rayleigh-Taylor instabilities (e.g. Elmegreen 1993, Vázquez-Semadeni et al. 2000 for an overview, or Burkert & Lin 2000 for an analysis of the thermal instability). Within the highly structured and dynamically active molecular cloud environment, stars form in groups and build up from gas that is subject to localized gravitational instability. The density in the central part of a collapsing gas clump increases enormously and a protostellar object forms. The nascent protostar grows in mass via accretion from the infalling envelope until the available gas reservoir is exhausted or stellar feedback effects become important and remove the parental cloud — a new star is born (for a comprehensive overview consult Mannings, Boss & Russell 2000, and references therein). This complex evolutionary sequence involves a wide variety of different physical phenomena, and it is not at all well understood which processes dominate and determine the spectrum of stellar masses and the kinematic and spatial properties of young star clusters.

The current investigation focuses on the initial phases of the star formation process. We model the fragmentation and dynamical evolution of large subvolumes within molecular clouds towards the formation of clusters of protostellar cores using smoothed particle hydrodynamics (SPH – see the reviews of Benz 1990 and Monaghan 1992) implemented with the special-purpose hardware device GRAPE (Sugimoto et al. 1990, Ebisuzaki et al. 1993). This extends previous studies of the collapse of isolated gas clumps (e.g. Burkert & Bodenheimer 1996; Burkert, Bate & Bodenheimer 1997; Boss 1997, Truelove et al. 1998, Bate 1998) to the molecular cloud regime and allows us to consistently and statistically study the formation process of stellar clusters within globally stable molecular clouds. Stellar cluster formation through gravitational collapse and fragmentation of isolated gas spheres has been modeled with low resolution by Larson 1978, and Keto, Lattanzio & Monaghan 1991. Star formation at the interface of colliding gas spheres has been studied by Whitworth et al (1995), Turner et al. (1995) and Bhattal et al. (1998), and the effect of gas accretion onto embedded young stellar clusters was discussed by Bonnell et al. (1997). The simulations presented here combine all these different aspects of star formation by self-consistently following the isothermal evolution of turbulent molecular clouds towards the formation of stellar clusters including its competitive accretion phase.

As we want to understand which physical effects determine the properties of stellar clusters and how these depend on different initial cloud conditions, we adopt the following approach: It is known from numerical studies that interstellar turbulence decays very rapidly, on time scales of the order of the free-fall time scale of molecular clouds (Gammie & Ostriker

1996, Mac Low et al. 1998, Stone, Ostriker & Gammie 1998, Mac Low 1999, Padoan & Nordlund 1999). This is also the typical time scale inferred for the formation of star clusters (e.g. Carpenter et al. 1997, Hillenbrand & Hartmann 1998, also Elmegreen 2000). Clustered star formation therefore occurs in molecular cloud regions which have (locally) lost their turbulent pressure support or, almost equivalently, which are only weakly supported by turbulence on large scales (Klessen, Heitsch & Mac Low 2000). The turbulent velocity field in the subvolume under consideration is assumed to leave a Gaussian fluctuation spectrum as imprint into the density distribution of the cloud. The dynamical evolution of the cloud in the isothermal phase is thus determined by two parameters, the power spectrum $P(k)$ of the fluctuations and the gas temperature. We consider power-law spectra $P(k) \propto k^{-\nu}$ with slopes ranging from $\nu = 0$ to $\nu = 3$ and gas temperatures such that the considered volume contains between 1 and 222 thermal Jeans masses. In the first part of this investigation (Klessen & Burkert 2000, in the following denoted Paper I; see also Klessen, Burkert, & Bate 1998) we presented the results of a detailed case study and focused on an in-depth analysis of the formation of stellar clusters in subregions containing 222 Jeans masses within clumpy molecular clouds with power spectrum $P(k) \propto k^{-2}$. Using some of the statistical tools introduced in Paper I, we discuss here selected aspects of the complete survey of the parameter space which we performed.

The results of Paper I showed that even simple, isothermal models of self-gravitating clumpy clouds are able to explain many of the observed features of star-forming regions. This is rather surprising, given the fact that magnetic fields and energetic heating processes of newly formed stars could in principle be important, both of which have been neglected. The early stages of star formation are dominated by the interplay between turbulence and gas pressure on one side and the gravitational forces on the other. This creates an intricate network of filaments, sheets and dense clumps. Some clumps will become gravitationally unstable and undergo rapid collapse. While contracting individually to form protostellar cores in their interior, gas clumps stream towards a common center of attraction. Throughout this paper, the terms gas clump and density fluctuation are used synonymously, cores are defined as the high-density central regions of collapsing clumps where individual protostars build up. As described in Section 2, the numerically unresolved cores are replaced by sink particles. Altogether, the dynamical evolution of molecular clouds involves processes acting simultaneously on different length scales and time scales. A quasi-equilibrium clump mass spectrum emerges and follows a power-law $dN/dM \propto M^{-1.5}$. Individual clumps are elongated, centrally condensed objects with 2:1 to 4:1 axis ratios and with r^{-2} density fall-off. In contrast to the clumps, the core mass spectrum is best described by a log-normal distribution with a peak and a width that is in excellent agreement with observations of multiple stellar systems.

The presence of unpredictable dynamical processes in the overall gas flow and the evolution of the nascent protostellar cluster very efficiently erases the memory of the initial configuration. For this reason, it is impossible to predict the detailed evolution of individual objects from the initial state of the system. Only the properties of an *ensemble* of protostellar cores, for example their kinematics and mass distribution, can be determined in a probabilistic sense. A comprehensive theory of star formation needs to be a statistical theory.

In the present part II, we investigate how the formation of protostellar clusters depends on variations in the environmental and initial conditions. The structure of the paper is as follows. First (in §2) we briefly recapitulate the properties of our numerical models as introduced in detail in Paper I, then we analyze (§3) the dependence of the dynamical evolution of the system on the slope ν of the initial fluctuation spectrum. We discuss the stability of the resulting core clusters in §4, and vary the temperature in §5. Finally, we summarize our results in §6.

2. Models

2.1. SPH in Combination with GRAPE

SPH (*smoothed particle hydrodynamics*) is a Lagrangian method to solve the equations of hydrodynamics. The fluid is represented by an ensemble of particles and thermodynamical observables are obtained by averaging over an appropriate subset of the SPH particles (Benz 1990, Monaghan 1992). The method is very flexible and able to resolve very high density contrasts by increasing the particle concentration where needed. We use SPH in combination with the special-purpose hardware device GRAPE (Sugimoto et al. 1990, Ebisuzaki et al. 1993), which allows calculations at supercomputer level on a normal workstation. In addition, we implemented periodic boundary conditions (Klessen 1997) to describe molecular clouds that are stable against gravitational collapse on global scales and to concentrate on the dynamical evolution of subvolumes within those clouds.

In any self-gravitating fluid, regions with masses exceeding the Jeans limit become unstable and collapse. In our implementation of SPH, once a highly-condensed object forms in the center of a collapsing gas clump and has passed beyond a certain density threshold, the dense core is substituted by a sink particle (Bate, Bonnell & Price 1995). The density limit is four to five orders of magnitude above the initial average density, depending on the particle number in the simulation, and the accretion radius of the sink particle is slightly larger than the corresponding Jeans length. The particle inherits the combined masses,

linear and relative angular momenta of the SPH particles it replaces, and has the ability to accrete further SPH particles from its infalling gaseous surrounding. Again, the mass, linear and angular momenta are conserved. By adequately replacing high-density cores by sinks and keeping track of their further evolution in a consistent way we are able to follow the dynamical evolution of the system over many free-fall times.

More details about the implementation of SPH which we use and its advantages and limitations of the method are discussed in §2 of Paper I.

2.2. Initial Conditions

We investigate the first phases of star formation, the dynamical evolution and fragmentation of structure within molecular clouds towards the formation of clusters of embedded accreting protostellar cores. In this regime the gas is approximately isothermal with a typical temperature of 10 K (e.g. Tohline 1982). Stellar clusters are known to form quickly on the order of the local collapse time scale (e.g. Hillenbrand & Hartmann 1998, Elmegreen 2000). This requires the coherent loss of turbulence within a sufficiently large molecular cloud region and we start our simulations at the onset of gravitational contraction. The initial density fluctuation spectra are taken to be Gaussian with power distribution $P(k) \propto k^{-\nu}$, with the exponents in the range $\nu = 0$ to $\nu = 3$. The velocity is computed self-consistently from the density by solving Poissons equation, i.e. the gas velocity at any location is due to gravitational contraction only, additional contribution from interstellar turbulence are assumed to have decayed away.

The slope $\nu = 0$ of the density spectrum implies equal power on all scales. As a result, the structure of the system appears relatively homogeneous without large-scale features. Such density structure is the imprint of turbulence that contained most energy on small scales. As the exponent ν increases, the fluctuation spectra become steeper and the spatial structure of the simulated molecular clouds volume become more and more dominated by large-scale modes. This effect is nicely illustrated in figure 1 at $t = 0$. Large-scale density fluctuations are assumed to stem from turbulent velocity fields that have been dominated by large-scale modes.

Assuming that stellar clusters form through the gravitational collapse of clumpy cloud regions that have lost their turbulent support, we study the detailed behavior of this process and the properties of the newly formed cluster. The current study does not include the possible effect of magnetic fields on this process. However, the overall importance of magnetic fields and MHD waves on the dynamical structure of molecular clouds may not be large. The

energy associated with the observed fields is of the order of the (turbulent) kinetic energy content of molecular cloud clumps, and smaller than the gravitational one (Crutcher 1999). Hence, the observed fields are too weak to prevent local collapse. In addition, the presence of magnetic fields cannot halt the decay of turbulence (Mac Low et al. 1998, Stone et al. 1998, Padoan & Nordlund 1999), and may not be able to significantly alter the efficiency of local collapse in the case of driven turbulence (Heitsch, Mac Low, & Klessen 2001). In the case of stable cloud regions external driving mechanisms are necessary, otherwise kinetic energy dissipates quickly in regions without driving sources, resulting in the rapid formation of stellar clusters. This is what we consider here. Star formation on a crossing time scale is implied by observational evidence also on scales of molecular clouds as a whole (Ballesteros-Paredes, Hartmann, & Vázquez-Semadeni 1999, Elmegreen 2000), again supporting the present model where magnetic fields does not play a dominant role.

We adopt random Gaussian fluctuations for the density as starting condition for the SPH simulations, because their properties resemble the end stages of decaying turbulence and are suited to mimic observed features of molecular clouds once advanced into the non-linear regime (see e.g. Stutzki & Güsten 1990, who deploy a Gaussian decomposition technique to describe the clumpy structure of molecular clouds). It is important for the current parameter study, that these distributions have well defined statistical properties. Gaussian random fields are completely characterized by the normalization and the power spectrum $P(\vec{k})$, i.e. all higher moments can be expressed in terms of the first two moments. In case of isotropy, the power distribution is independent of direction and depends only on the wave number $k = |\vec{k}|$. The function $P(k)$ identifies the contribution of waves with wave number k to the statistical fluctuation spectrum. The phases of Gaussian random fields are arbitrarily chosen from a *uniform* distribution in the interval $[0, 2\pi[$, and the amplitudes for each mode k are randomly drawn from a *Gaussian* distribution with width $P(k)$ centered on zero. Since waves are generated from random processes, only the properties of an *ensemble* of fluctuation fields are determined in a statistical sense. Individual realizations (from different sets of random numbers) may deviate considerably from this mean value, especially at small wave numbers k . We generate the initial density fluctuation fields by applying the Zel’dovich (1970) approach. The method and its applicability to gaseous systems is discussed in detail in §3 and Appendix B of Paper I.

2.3. Scaling Properties

For isothermal gas, the energy density is a function of temperature only and the equation of state reduces to $p = c_s^2 \rho$, with c_s being the thermal sound speed. The self-gravitating,

isothermal model studies the interplay between gravity and gas pressure. Given the initial density and velocity distribution, i.e. a slope ν of the density fluctuation spectrum, the dynamical evolution of the system depends only on one free scaling parameter, the ratio α between the total internal energy ϵ_{int} and the total potential energy ϵ_{pot} in the system, which is equivalent to a dimensionless *temperature*,

$$\alpha \equiv \epsilon_{\text{int}}/|\epsilon_{\text{pot}}|. \quad (1)$$

Generally, all physical parameters and constants in our models are normalized and set to unity. The same applies to mass and length scales. The total mass in the system is $M = 1$ and the simulated volume is the cube $[-1, +1]^3$, i.e. the mean density is $\langle \rho \rangle = 1/8$. In these units the thermal Jeans mass for spherical perturbations is

$$M_{\text{J}} = 1.6 \cdot \rho^{-1/2} \alpha^{3/2}. \quad (2)$$

Using the average value $\langle \rho \rangle = 1/8$ for the density, the global free-fall time is $\tau_{\text{ff}} = 1.5t$ with t being the dimensionless time unit. The parameter α regulates the number of thermal Jeans masses contained within the simulated volume, $N_{\text{J}} = 1/M_{\text{J}}$. We vary the dimensionless temperature from $\alpha = 0.01$ to $\alpha = 0.5$. In Paper I we considered $\alpha = 0.01$, which corresponds to $N_{\text{J}} = 222$ and leads to the formation of clusters of ~ 60 protostars. A value $\alpha = 0.5$ implies $N_{\text{J}} = 0.6$. Collapse does not occur. When increasing the scaling parameter α , the total number of Jeans masses contained in the computed cube decreases. In the isothermal models this is equivalent to ‘zooming’ in onto smaller spatial volumes. By this, individual protostellar clumps are better resolved with the caveat of neglecting the influence of modes with wave lengths larger than the box size.

To illustrate the corresponding physical scaling, we consider sites of low-mass star formation, like Taurus, with $n(\text{H}_2) \approx 10^2 \text{ cm}^{-3}$ and $T \approx 10 \text{ K}$. Assuming a mean molecular weight of $\mu = 2.36$, for $\alpha = 0.01$ the simulated cube contains the mass $M = 6\,300 M_{\odot}$ and has a size $L = 10.2 \text{ pc}$. For $\alpha = 0.5$ the volume is much smaller with $M = 17.4 M_{\odot}$ and $L = 1.44 \text{ pc}$. The time unit is equivalent to $t = 2.2 \times 10^6$ years and the average Jeans mass transforms to $M_{\text{J}} = 28 M_{\odot}$. When applied to dense, massively star-forming clouds with typically $n(\text{H}_2) \approx 10^5 \text{ cm}^{-3}$ and $T \approx 10 \text{ K}$, similar to the BN region in Orion, the simulated cube translates into the mass $M = 200 M_{\odot}$ and the size $L = 0.32 \text{ pc}$ for $\alpha = 0.01$ and $M = 0.6 M_{\odot}$ and the size $L = 0.05 \text{ pc}$ for $\alpha = 0.5$. The time unit now converts to $t = 7.0 \times 10^4$ years and the mean Jeans mass for the homogeneous distribution is $M_{\text{J}} = 0.9 M_{\odot}$.

3. Dependence on the Power Spectrum

In this section we analyze the dependence of the fragmentation of a region inside a molecular cloud and of the properties of the protostellar cluster that forms during the dynamical evolution on the choice of the initial fluctuation spectrum $P(k) \propto 1/k^\nu$. Again for models with $\alpha = 0.01$ which contain 222 Jeans masses, we compare the evolution of the system for different values of ν , ranging from $\nu = 0$ which means that fluctuations of all wave lengths k have statistically the same amplitude, to the very steep power spectrum $\nu = 3$ which implies strong dominance of the large-scale modes. For $\nu = 0$, the initial density distribution looks quite homogeneous, whereas it is strongly biased towards having one dominant density peak in the case of $\nu = 3$. Additionally, for $\nu = 1$ we study the case of a truncated spectrum where fluctuations on scales $k < 4$ have been removed. For a comparison of the initial density fields with different power spectra see Fig. 1. The parameters of all models discussed in this section are listed in Tab. 1.

3.1. Dependence on the Slope of the Power Spectrum

To examine how the variation of the slope ν of the initial fluctuation spectrum influences the dynamical evolution of the gas system, we generate four models with varying ν but otherwise almost identical properties. Models $\mathcal{A}0a$, $\mathcal{A}1a$, $\mathcal{A}2a$ and $\mathcal{A}3a$ have $\nu = 0$, $\nu = 1$, $\nu = 2$ and $\nu = 3$, respectively. All consist of 2×10^5 SPH particles and are generated via the Zel’dovich method from the same initial random particle distribution, applying the same shift interval $\delta t = 1.5$. To exclude the variance effects inevitable when comparing different realizations of a fluctuation field with given statistical properties, models $\mathcal{A}0a$, $\mathcal{A}1a$ and $\mathcal{A}3a$ are computed from the same set of random numbers used to generate the fluctuation spectrum. This means, that individual modes k in each of the three fields have identical *phases*. However, they differ in *amplitude*, since these are drawn from Gaussians with different width $P(k) \propto 1/k^\nu$, where $\nu = 0, 1$ or 3 , respectively. For this reason, at comparable stages of their dynamical evolution, the three models look remarkably similar. For model $\mathcal{A}2a$ a different set of random numbers is used, and statistical variance leads to a different appearance. This can be seen in Fig. 1, which plots the 3-dimensional particle distribution for each model at different stages of the dynamical evolution. The first row denotes model $\mathcal{A}0a$, the second row model $\mathcal{A}1a$, the third one model $\mathcal{A}2a$ and finally the fourth row model $\mathcal{A}3a$. Each column in the figure shows the distributions at comparable evolutionary phases, characterized by the mass fraction M_* accreted onto protostellar cores, as indicated at the top of each column. The first column shows the initial density distribution, the second column describes the state of the system when the maximum density contrast

has reached half the value necessary for a collapsing object to be identified as protostellar core (see Sec. 2.1), the third column shows the system when 2% of the gas mass is contained in condensed cores, and so forth.

The overall dynamical evolution of all models is very similar: The cloud develops a complex filamentary structure, and dense cores form typically at the intersection of filaments. They accrete from the surrounding gas while streaming towards the common center of attraction. It is common to all models to form *clusters of protostellar cores which grow in mass via competitive accretion from the common gas reservoir*, as discussed in detail in Paper I.

However, there are differences in the detailed behavior. It is visible in the left column of Fig. 1 that steeper spectral slopes ν lead to initial density distributions that exhibit more spatial structure and higher degrees of inhomogeneity. The density fields of the models with $\nu \gtrsim 2$ are dominated by the largest-scale modes. On the other hand, for $\nu \lesssim 1$, fluctuations on smaller scales have sufficient amplitudes to compensate the large-scale fluctuations when the whole spectrum is added up, hence, model $\mathcal{A}0a$ (with $\nu = 0$) appears relative homogeneous initially. All initial fluctuation fields are generated using the Zel’dovich method with constant shift interval $\delta t = 1.5$. As discussed in Appendix B of Paper I, this implies that the initial density contrast increases with slope ν , lying between $\delta\rho/\rho = 3$ for $\mathcal{A}0$ and $\delta\rho/\rho = 50$ for $\mathcal{A}3$. Regions of higher density contrast begin to contract faster and the system reaches a given evolutionary stage at earlier times, since the free-fall time is a function of density, $\tau_{\text{ff}} \propto \rho^{-1/2}$. Compared to model $\mathcal{A}3a$ with the largest initial density contrast, model $\mathcal{A}0a$ lags behind by $\Delta t \approx 2.5$, model $\mathcal{A}1a$ by $\Delta t \approx 1.5$ and model $\mathcal{A}2a$ by $\Delta t \approx 1.0$. Despite this initial lag, the dynamical evolution runs synchronously, i.e. the time intervals between different stages of star formation are comparable in all models. The overall age spread between the appearance of the first and the last identified cores is roughly 1.3 free-fall times τ_{ff} .

The slope of the power spectrum and the initial density contrast also influences the total number of protostellar cores that form during the dynamical evolution. If superposed on large-scale density modes, the probability of small-scale fluctuations to exceed the local Jeans limit is increased by the contribution of the large-scale mode, since $M_{\text{J}} \propto \rho^{-1/2}$ (Eqn. 2). This effect is not large for models $\mathcal{A}0a$ to $\mathcal{A}2a$, they all form between 45 and 59 cores, but becomes important for model $\mathcal{A}3a$. It forms altogether 130 sinks.

The mass distribution of identified gas clumps and protostellar cores at comparably evolutionary stages are very similar. This can be seen in Fig. 2, which plots the number of gas clumps (thin lines) and of protostellar cores (thick lines) as function of their mass. Individual masses are scaled relative to the Jeans mass of the homogeneous cube which is $M_{\text{J}} = 1/222$. Analogous to Fig. 1, each row denotes an individual model (from $\nu = 0$ to

$\nu = 3$) and each column indicates the same evolutionary phases as in the previous figure. The vertical line denotes the SPH resolution limit, below which the local Jeans mass is not resolved properly (see Bate & Burkert 1997). The dashed line indicates the observed slope of the clump-mass spectrum $dN/dm \propto m^{-1.5}$.

Clearly, the initial conditions fail to reproduce the observed clump-mass distribution. Our clump-finding algorithm detects the initial Gaussian fluctuation spectrum and the clump spectra for the different models appear identical since the algorithm is biased towards small scale fluctuations: if a variety of small-scale peaks are superposed on a large-scale mode, it breaks the latter one up into the contributions of the smaller fluctuations. The large mode is identified only if it is sufficiently ‘smooth’, i.e. if it cannot be identified as the sum of an ensemble of smaller clumps. The algorithm is similar to the one described by Williams, De Geus, & Blitz (1994) adopted to make use of the SPH kernel smoothing and thus differs from the Gaussian decomposition scheme introduced by Stutzki & Güsten (1990). For a detailed description see Appendix A in Paper I.

As the system begins to evolve, gas pressure leads to the disintegration of small clumps with masses below a Jeans mass, whereas gravitational attraction causes more massive clumps to merge thus creating larger ones with increasing mass. As a result, for models $\mathcal{A}0a$ and $\mathcal{A}1a$, the clump spectrum becomes flatter in the interval $M_* \approx 1\%$ to $M_* \approx 30\%$. At later stages, additional low-mass clumps are identified which may result from irregularities or sub-fragmentation in the converging gas flows at the intersection of two filaments along which gas streams towards a common center of attraction (see Paper I for more details of this processes). At very late stages, when almost all mass is contained in protostellar cores, fitting a single power-law slope to the mass spectrum becomes completely meaningless. Since the models $\mathcal{A}2a$ and $\mathcal{A}3a$ pass through all evolutionary stages at earlier times, self-gravity and gas pressure have less time to shape the clump-mass spectrum. Therefore, these systems contain more low-mass clumps compared to the other two runs and their clump-mass spectrum is on average steeper. Again at late stages the distribution can no longer be fitted by a simple power law.

In summary, the clump-mass spectrum of self-gravitating isothermal gas evolves in time and exhibits a well defined power-law behavior only during the intermediate stages of its dynamical evolution. During this period, the slopes vary dN/dM gradually from values of about -1 to -2 . This is consistent with the variety of different slopes quoted for observed clump-mass spectra and the uncertainty in their determination (e.g. Stutzki & Güsten 1990, Williams et al. 1994, Kramer et al. 1998).

The mass distribution of protostellar cores is approximately log-normal covering two orders of magnitude in mass. It peaks roughly at the *mean Jeans mass* of the system. This

is in agreement with the results of Paper I and results from the fact that the formation of new low-mass protostellar cores and the accretion onto already existing ones are approximately in balance; they populate the low-mass and high-mass side of the distribution more or less equally. The peak of the distribution moves away from the Jeans mass only at late stages of the evolution, when the formation of new cores has stopped, but the already existing ones are still able to grow in mass. This effect is largest for model $\mathcal{A}0a$, since it forms the lowest total number of condensed cores. Model $\mathcal{A}3a$ builds up three times more cores. Therefore, each protostellar core is on average three times lighter than in the other cases and the distribution peaks at smaller masses. Only towards the end of the simulation, when almost all gas is accreted onto the protostellar cores the peak reaches values of the average Jeans mass.

3.2. Dependence on the Maximum Wave Number

The initial conditions for the SPH simulations are determined by the slope of the initial fluctuation spectrum. Furthermore, they depend on the number of modes that contribute to the overall fluctuation field. The initial fluctuations discussed so far are all generated from waves with $k = 1$, where the wave length is equal to the total size of the considered volume, down to $k = 32$, where the wave fits 32 times into the considered cube. For steep power spectra, the overall appearance of the fluctuation field is strongly dominated by the presence of the largest-scale modes (see Fig. 1). To investigate the importance of these modes on the evolution, model $\mathcal{A}1b$ has a initial a fluctuation spectrum truncated for modes $k < 4$ with slope $\nu = 1$. It is generated with a Zel’dovich shift interval $\delta t = 1.0$.

The time evolution of the system is displayed in Fig. 3, which shows the particle distribution at different stages of the dynamical evolution characterized by the total mass fraction M_* accumulated in protostellar cores. Since the Zel’dovich shift interval is relatively small and the initial fluctuation field lacks the presence of large-scale modes, the particle distribution appears very smooth and homogeneous. Its evolution is most comparable to model $\mathcal{A}0a$, which also is very homogeneous and smooth at the beginning of the evolution. The initial density contrast in model $\mathcal{A}1b$ is even smaller than in model $\mathcal{A}0a$, which implies that it needs longer to reach comparable evolutionary stages, e.g. it takes $t \approx 3.9$ to form the first highly-collapsed protostellar object. However, as in all other models, a bound cluster of protostellar cores builds up. Again, the mass spectrum is very broad, spanning two orders of magnitude, and peaks slightly above the mean Jeans mass as derived from the mean density; the mass spectrum of protostellar cores is indistinguishable from the one of model $\mathcal{A}0a$.

In summary, removing the large-scale modes is equivalent to flattening the overall spectral slope. The details depend on the slope of the initial spectrum and the wave number

up to which fluctuations are deactivated. Removing all modes with $k < 4$ in a model with $\nu = 1$ produces a system that in many aspects behaves like a model with $\nu = 0$.

4. The Dynamical Stability of the Protostellar Cluster

Figure 4 specifies the energy and kinematic properties of the protostellar cluster that forms in each of the above models. In (a) the time evolution of the kinetic energy of the random motions of the protostellar cores is plotted, $E_{\text{int}} = 1/2 \sum_i m_i (\vec{v}_i - \vec{v}_{\text{cm}})^2$, where m_i and \vec{v}_i are the masses and velocities of individual cores i , and $\vec{v}_{\text{cm}} = \sum_i m_i \vec{v}_i / M_*$ is the center-of-mass velocity of the protostellar cluster. In (b) the potential energy of the cluster disregarding the contribution from the surrounding gas is shown, $E_{\text{pot}} = \sum_{ij} G m_i m_j / r_{ij}$, with the gravitational constant set to unity. The distance between two cores i and j is denoted $r_{ij} = |\vec{r}_i - \vec{r}_j|$, where each pair is counted once. The velocity dispersion $\sigma^2 = \sum_i (\vec{v}_i - \vec{v}_{\text{cm}})^2$ and the total mass accumulated in protostellar cores $M_* = \sum_i m_i$ are specified in (c) and (d), respectively. In Fig. 4 and also in Fig. 5, open diamonds denote model $\mathcal{A}0a$ with $\nu = 0$, and triangles the models with $\nu = 1$, $\mathcal{A}1a$ (open symbols) and the high-resolution model $\mathcal{A}1b$ (filled symbols), whose initial fluctuation spectrum is truncated at large scales, i.e. contains only modes with $4 \leq k$. The two models with $\nu = 2$, $\mathcal{A}2a$ and $\mathcal{A}2b$ are plotted with open and filled circles, respectively. Finally, the model with the steepest initial fluctuation spectrum (with $\nu = 3$) is given by open squares. From Fig. 4, one immediately reads off the different time delays for models with the different spectral slopes ν . Furthermore, one sees that the evolution of the energetic and kinematic properties of the cluster in model $\mathcal{A}2a$ and $\mathcal{A}2b$ is almost identical, independent of their different particle number (as discussed in detail in Paper I). The delay between the two models with $\nu = 1$, $\mathcal{A}1a$ and $\mathcal{A}1b$, is due to the truncation of the initial fluctuation spectrum of $\mathcal{A}1b$ as discussed in § 3.2.

Figure 5, specifies the time evolution of the virial coefficient, $\eta_{\text{vir}} = 2E_{\text{int}}/|E_{\text{pot}}|$. This quantity is obtained from core properties only. The contribution of the remaining gas in the cluster region is not included since we want to estimate the possible dynamical evolution of the cluster *after* a possible gas removal. A value $\eta_{\text{vir}} = 1$ suggests that the cluster is in virial equilibrium, $\eta_{\text{vir}} < 1$ indicates that gravitational attraction outweighs kinetic energy and the cluster is contracting, and in the case $\eta_{\text{vir}} > 1$ the cluster will be expanding if the gas gets removed. To compare the virial coefficient of each model at comparable evolutionary stages, Fig. 5e plots η_{vir} as function of the total fraction of gas converted into protostellar cores M_* . Finally, Fig. 5f specifies the average value and its uncertainty. The scatter at early times or equivalently at very low values of M_* is due to the small number statistics. As more and more protostellar cores form, they follow the global gas flow towards the common center of

gravity, where they build up an embedded dense cluster. For simulations with an initial $\nu = 2$ -fluctuation spectrum this has been discussed in detail in Paper I. Our simulations show that the nascent protostellar clusters are bound even without the gravitational contribution of the gas. The conversion of gas into dense cores proceeds such that the overall gain of potential energy is more or less balanced by the increase of kinetic energy. However, due to the limited available gas reservoir, the virial coefficient increases slowly with time in this conversion process. This is best seen in Fig. 5f. At the time when the gas reservoir is completely depleted the virial coefficient is $\eta_{\text{vir}} \simeq 0.6$. Now the clusters behave like collision-dominated N -body systems and develop a characteristic core/halo structure with the virial coefficient approaching unity. The overall velocity dispersion σ and the energies E_{int} and $|E_{\text{pot}}|$ decrease again (as visible in the evolution of model $\mathcal{A}2a$ in Fig. 4, open circles).

The situation becomes more complicated, when the subsequent collapse of cores into individual stars is considered. Whereas the cluster of protostellar cores is a bound entity, this may no longer be true for the resulting *stellar* cluster. If the star-formation efficiency of individual cores is very low, a large fraction of the gas accumulated in the protostellar core is expelled again (i.e. in protostellar outflows) and will not end up in the stars. If this mass-loss occurs rapidly, the resulting star cluster retains the original velocity dispersion, while its potential becomes shallower due to this mass loss, and as a consequence, the cluster dissolves. Only for small or gradual mass loss can the system expand adiabatically and remain bound (Geyer & Burkert 2000). Observations (Motte, André and Neri 1998, P. André private communication) and detailed numerical collapse simulations (Wuchterl & Tscharnuter 2000, Wuchterl & Klessen 2000), however, indicate that most of the matter that gets accumulated in protostellar cores actually continues to accrete onto the central protostellar object. Hence, our current set of simulations is indeed indicative about the dynamical fate of the resulting stellar cluster.

5. Dependence on the Temperature

For a given density, the Jeans mass is a function of the temperature of the isothermal gas (Eqn. 2). Changing the temperature modifies the number of Jeans masses contained in simulation. Since the isothermal models can be scaled to a wide range of physical regimes, increasing the dimensionless temperature, i.e. the scaling parameter α , but keeping the physical gas temperature constant (say at 10K) is equivalent to zooming in more closely onto smaller physical scales. Vice versa, decreasing the scaling parameter implies to study a larger volume of molecular cloud material. For example, the behavior of systems with dimensionless temperatures $\alpha = 0.04$ is comparable to the dynamical evolution within sub-

regions of volume $1/8$ in a model with $\alpha = 0.01$ (i.e. in one octant of the simulation cube). This, however, neglects the influence of large-scale modes that are present in the simulations of larger volumes, and the approximation is only good for the first stages of the evolution. All simulations show that after one or two global free-fall times the overall matter distribution is determined by the growth of the largest possible mode in the system. There is always *one* global minimum of the potential, towards which the bulk of matter flows, leading to the formation of *one* protostellar cluster. The (periodic) boundary conditions of a model with high temperature are not identical with the boundary conditions of a subregion within a model with lower temperature, which contains a comparable number of Jeans masses. As the time progresses in both systems, the influence of the boundary conditions on the dynamical evolution increases. At late times, deviations between both models are expected and detailed comparison becomes less meaningful. Properties of the system that are strongly influenced by large-scale flows and are the result of considerable dynamical evolution are expected to be different, e.g. the spatial properties of the forming protostellar clusters. Properties that are less sensitive to these processes, e.g. the overall slope of the clump-mass spectrum, are comparable in both models at all times. This is true for the evolution of the mass spectrum which is dominated by local processes, by the interplay between gravitational attraction and gas pressure.

To quantify the temperature dependence (i.e. the dependence on the ratio of gravity forces to gas pressure forces), we perform a series of simulations with varying temperature parameter α , as listed in Tab. 2. All models contain 5×10^4 particles with different slopes of the initial fluctuation spectrum. We consider $\nu = 1$ and $\nu = 2$. The covered temperature parameters range from $\alpha = 0.01$, corresponding to 222 Jeans masses, to $\alpha = 0.5$, which means the Jeans mass is larger than the mass contained in the cube. Figure 6 specifies the total number N_* of protostellar cores that form during the dynamical evolution as function of the temperature α (lower abscissa) or equivalently the number N_J of Jeans masses in the system (upper abscissa). To indicate the power-law behavior of the dependence of N on α , the inlay shows $N(\alpha)$ in a log-log plot. In the models with temperatures $\alpha \gtrsim 0.25$ no fluctuations are massive enough in order to exceed the Jeans limit. All initial density fluctuations are smeared out by pressure forces and the system reaches a state of maximum homogeneity. Collapse occurs only for models with lower temperatures or, equivalently, regions that contain a sufficient number of Jeans masses. The number of forming protostellar cores scales roughly *linearly* with the number of Jeans masses in the system $N \propto N_J$ or equivalently $N \propto \alpha^{-3/2}$. With our definition of the Jeans mass (Eqn. 2) one core typically forms for every four Jeans masses.

We find as a general feature of all our simulations of regions within molecular clouds which have lost their turbulent support that their subsequent dynamical evolution leads to

the formation a cluster of protostellar cores with a wide mass distribution. The protostellar mass spectrum typically spans two orders of magnitude and always peaks around the *average Jeans mass* of the system. All of our simulation cloud regions exhibit this behavior as long as they are sufficiently massive to be able to form a cluster of stars. This is *independent* of the adopted initial fluctuation spectrum. This may seem somewhat surprising, as individual protostellar cores form and grow in mass via a sequence of highly *stochastic* events (Paper I). They form and feed from gas clumps and fluctuations of widely different masses, sizes and density contrasts, each leading to different collapse times and length scales. However, in a statistical sense the overall dynamical evolution progresses such that the system retains knowledge of its average properties (density and temperature). Our numerical simulations therefore support the hypothesis (e.g. Larson 1978, 1985) the *average Jeans mass* is the main parameter that determines the peak of the IMF.

6. Summary

We have performed hydrodynamic simulations of the dynamical evolution and fragmentation of regions within molecular clouds which have lost their turbulent support leading to gravitational contraction. As the most general approach which allows for an adequate description of the statistical properties we have assumed that the density field imprinted by the fading turbulent velocity field is described by random Gaussian fluctuations. We vary the slope ν of the power spectrum of the fluctuation field $P(k) \propto k^{-\nu}$ and the number of Jeans masses contained in the considered volume. Spectra with steep slopes ($\nu = 3$) correspond to initial matter distributions that are highly fragmented and exhibit large density contrasts. These systems are dominated by large-scale modes. In the case of flat spectra ($\nu = 0$), all spatial modes contribute equally to the density field. Consequently, these systems appear more or less homogeneous and exhibit no strong density contrasts. In Paper I we concentrated on a detailed analysis of the case $\nu = 2$. Here, we discussed the complete set of simulations with slopes ranging from $\nu = 0$ to 3 and we considered molecular cloud volumes that contain a wide range of different masses relative to the average Jeans mass (from $1 M_J$ to $222 M_J$).

The dynamical evolution of the simulated molecular cloud regions is rather insensitive to the slope of the initial density fluctuation spectrum. On a relatively short time scale, i.e. within one or two free-fall times, the system evolves into a complex network of intersecting filaments and collapsing clumps leading to the formation of a compact cluster of accreting and interacting embedded protostellar cores. These clusters form as bound entities, with central densities being roughly a few 10^2 times larger than the initial average gas density. In

their later phase of evolution, however, the clusters dissolve due to close encounters between the protostars (as discussed in more detail in Paper I).

In *all* simulations, the mass spectrum of collapsed cores is very broad, has approximately log-normal shape and peaks roughly at the average Jeans mass. This is independent of the adopted initial conditions. The number of protostellar cores that form is linearly proportional to the number of thermal Jeans masses in the studied region. Despite the fact that individual cores evolve through a sequence of highly stochastic events, in a statistical sense the evolution retains knowledge of the mean properties of the system. This supports the hypothesis that the average Jeans mass is the main parameter determining the peak in the stellar spectrum.

The current investigation and the detailed analysis presented in Paper I demonstrates good agreement between the current isothermal fragmentation model and the properties of observed star forming regions. This is somewhat surprising given the fact that we have neglected magnetic fields, energetic feedback processes or external environmental effects. It indicates that the interplay between self-gravity on the one side and thermal and turbulent pressure on the other side is the dominant process that regulates the formation of stellar clusters.

We thank Rainer Spurzem and Pavel Kroupa for many discussion on stellar clusters, and the anonymous referee for detailed comments.

REFERENCES

- Ballesteros-Paredes, J., Hartmann, L., Vázquez-Semadeni, E. 1999a, *ApJ*, 527, 285
- Bate, M. R., 1998, *ApJ*, 508, L95
- Bate, M.R., Bonnell, I.A, Price, N.M. 1995, *MNRAS*, 277, 362
- Bate, M.R., Burkert, A., *MNRAS*, 288, 1060
- Benz, W., 1990, in *The Numerical Modelling of Nonlinear Stellar Pulsations*, ed. J. R. Buchler, p. 269, Kluwer Academic Publishers, The Netherlands
- Bhattal, A. S., Francis, N., Watkins, S. J., Whitworth, A. P., 1998, *MNRAS*, 297, 435
- Bonnell, I. A., Bate, M. R., Clarke, C. J., Pringle, J. E., 1997, *MNRAS*, 285, 201
- Boss, A. P., 1997, *ApJ*, 483, 309
- Burkert, A., Bate, M. R., Bodenheimer, P., 1997, *MNRAS*, 289, 497

- Burkert, A., Bodenheimer, P., 1996, MNRAS, 280, 1190
- Burkert, A., Lin, D. N. C., 2000, ApJ, 537, 270
- Carpenter, J. M., Meyer, M. R., Dougados, C., Strom, S. E., Hillenbrand, L. A.: 1997. AJ, 114, 198
- Crutcher, R. M. 1999, ApJ, 520, 706
- Ebisuzaki, T., Makino, J., Fukushige, T., Taiji, M., Sugimoto, D., Ito, T., Okumura, S. K., 1993, PASJ, 45, 269
- Elmegreen, B. G., 1993, in Protostars and Planets III, eds. E. H. Levy, J. I. Lunine, Tucson, University of Arizona Press, p. 97
- Elmegreen, B. G., 2000, ApJ, 530, 277
- Gammie, C. F., Ostriker, E. C., 1996, ApJ, 466, 814
- Geyer, M., Burkert, A., 2000, ApJ, in preperation
- Heitsch, F., Mac Low, M.-M., Klessen, R. S., 2001, ApJ, in press
- Hillenbrand, L. A., Hartmann, L. W., 1998, ApJ, 492, 540
- Keto, E. R., Lattanzio, J. D., Monaghan, J. J., 1991, ApJ, 383, 639
- Klessen, R. S., 1997, MNRAS, 292, 11
- Klessen, R. S., Burkert, A., 2000, ApJS, 128, 287 (Paper I)
- Klessen, R. S., Burkert, A., Bate, M. R., 1998, ApJ, 501, L205
- Klessen, R. S., Heitsch, F., Mac Low, M.-M., 2000, ApJ, 535, 887
- Kramer, C., Stutzki, J., Rohrig, R., Corneliussen, U., 1998, A&A, 329, 249
- Larson, R. B., 1978, MNRAS, 184, 69
- Larson, R. B., 1985, MNRAS, 214, 379
- Mac Low, M.-M., 1999, ApJ, 524, 169
- Mac Low, M.-M., Klessen, R. S., Burkert, A., Smith, M.D., 1998, Phys. Rev. Lett., 80, 2754
- Mannings, V., Boss, A., Russell, S. (eds.), 2000, Protostars and Planets IV, University of Arizona Press, Tucson
- Monaghan, J. J., 1992, ARA&A, 30, 543
- Motte, F., André, P., Neri, R., 1998, A&A, 336, 150
- Padoan, P., Nordlund, Å. 1999, ApJ, 526, 279
- Stone, J. M., Ostriker, E. C., Gammie, C. F. 1998, ApJ, 508, L99

- Stutzki, J., Güsten, R., 1990, *ApJ*, 256, 513
- Sugimoto, D., Chikada, Y., Makino, J., Ito, T., Ebisuzaki, T., Umemura, M., 1990, *Nature*, 345, 33
- Tohline, J. E., 1982, *Fund. of Cosmic Physics*, 8, 1
- Truelove, J. K., Klein, R. I., McKee, C. F., Holliman, J. H., Howell, L. H., Greenough, J. A., Woods, D. T.: 1998. *ApJ*, 495, 821
- Turner, J.A., Chapman, S.J., Bhattal, A.S., Disney, M.J., Pongracic, H., Whitworth, A.P., 1995, *MNRAS*, 277, 705
- Vázquez-Semadeni, E., Ostriker, E. C., Passot, T., Gammie, C. F., Stone, J. M., 2000, in *Protostars and Planets IV*, eds. V. Mannings, A. P. Boss, S. S. Russell, Tucson, University of Arizona Press, p. 3
- Whitworth, A. P., Chapman, S. J., Bhattal, A. S., Disney, M. J., Pongracic, H., Turner, J. A., 1995, *MNRAS*, 277, 727
- Williams, J. P., De Geus, E. J., Blitz, L., 1994, *ApJ*, 428, 693
- Wuchterl, G., Klessen, R. S., 2000, submitted to *Nature*

Table 1: Models with parameter $\alpha = 0.01$ and different initial power spectra $P(k) \propto k^{-\nu}$ with $\nu = 0 \dots 3$.

Model Name ^a	Power-Law Exponent	Temperature Parameter	Number of Jeans Masses ^b	Particle Number	Number of Collapsed Cores
$\mathcal{A}0a$	$\nu = 0$	$\alpha = 0.01$	$N_J = 222$	$N = 2 \times 10^5$	$N_* = 45$
$\mathcal{A}1a$	$\nu = 1$	$\alpha = 0.01$	$N_J = 222$	$N = 2 \times 10^5$	$N_* = 49$
$\mathcal{A}1b^c$	$\nu = 1$	$\alpha = 0.01$	$N_J = 222$	$N = 5 \times 10^5$	$N_* = 51$
$\mathcal{A}2a^d$	$\nu = 2$	$\alpha = 0.01$	$N_J = 222$	$N = 2 \times 10^5$	$N_* = 59$
$\mathcal{A}2b^d$	$\nu = 2$	$\alpha = 0.01$	$N_J = 222$	$N = 5 \times 10^5$	$N_* = 56$
$\mathcal{A}3a$	$\nu = 3$	$\alpha = 0.01$	$N_J = 222$	$N = 2 \times 10^5$	$N_* = 130$

^a The initial stages of all models have been generated with the Zel’dovich method from a random homogeneous field using $\delta t = 1.5$ (for details see Paper I).

^b Number N_J of thermal Jeans masses derived from the average density in the simulated cube.

^c The initial density distribution contains no large-scale modes, the fluctuation spectrum used to generate this model is truncated for wave numbers $k < 4$.

^d These two models are equivalent to models \mathcal{H} and \mathcal{I} in Paper I.

Table 2: Models with initial power spectra $P(k) \propto k^{-\nu}$, where $\nu = 0$ and $\nu = 2$, but different temperature parameters α .

Model Name ^a	Power-Law Exponent	Temperature Parameter	Number of Jeans Masses ^b	Particle Number	Number of Collapsed Cores
<i>B1a</i>	$\nu = 1$	$\alpha = 0.010$	$N_J = 222$	$N = 5 \times 10^4$	$N_* = 45$
<i>B1b</i>	$\nu = 1$	$\alpha = 0.025$	$N_J = 56$	$N = 5 \times 10^4$	$N_* = 15$
<i>B1c</i>	$\nu = 1$	$\alpha = 0.075$	$N_J = 11$	$N = 5 \times 10^4$	$N_* = 3$
<i>B1d</i>	$\nu = 1$	$\alpha = 0.100$	$N_J = 7$	$N = 5 \times 10^4$	$N_* = 1$
<i>B1e</i>	$\nu = 1$	$\alpha = 0.500$	$N_J < 1$	$N = 5 \times 10^4$	$N_* = 0$
<i>C1a</i> ^c	$\nu = 2$	$\alpha = 0.010$	$N_J = 222$	$N = 5 \times 10^4$	$N_* = 57$
<i>C1b</i>	$\nu = 2$	$\alpha = 0.025$	$N_J = 56$	$N = 5 \times 10^4$	$N_* = 21$
<i>C1c</i>	$\nu = 2$	$\alpha = 0.050$	$N_J = 20$	$N = 5 \times 10^4$	$N_* = 13$
<i>C1d</i>	$\nu = 2$	$\alpha = 0.250$	$N_J = 2$	$N = 5 \times 10^4$	$N_* = 6$
<i>C1e</i>	$\nu = 2$	$\alpha = 0.500$	$N_J < 1$	$N = 5 \times 10^4$	$N_* = 0$

^a The initial stages of all models have been generated with the Zel’dovich method from a random homogeneous field. For models *B1d* and *B1e* a shift interval $\delta t = 1.0$ is used. For *C2a* it is $\delta t = 2.0$ and for all other ones $\delta t = 1.5$ (for details see Paper I).

^b Number N_J of thermal Jeans masses derived from the average density in the simulated cube.

^c This model corresponds to model *A* in Paper I.

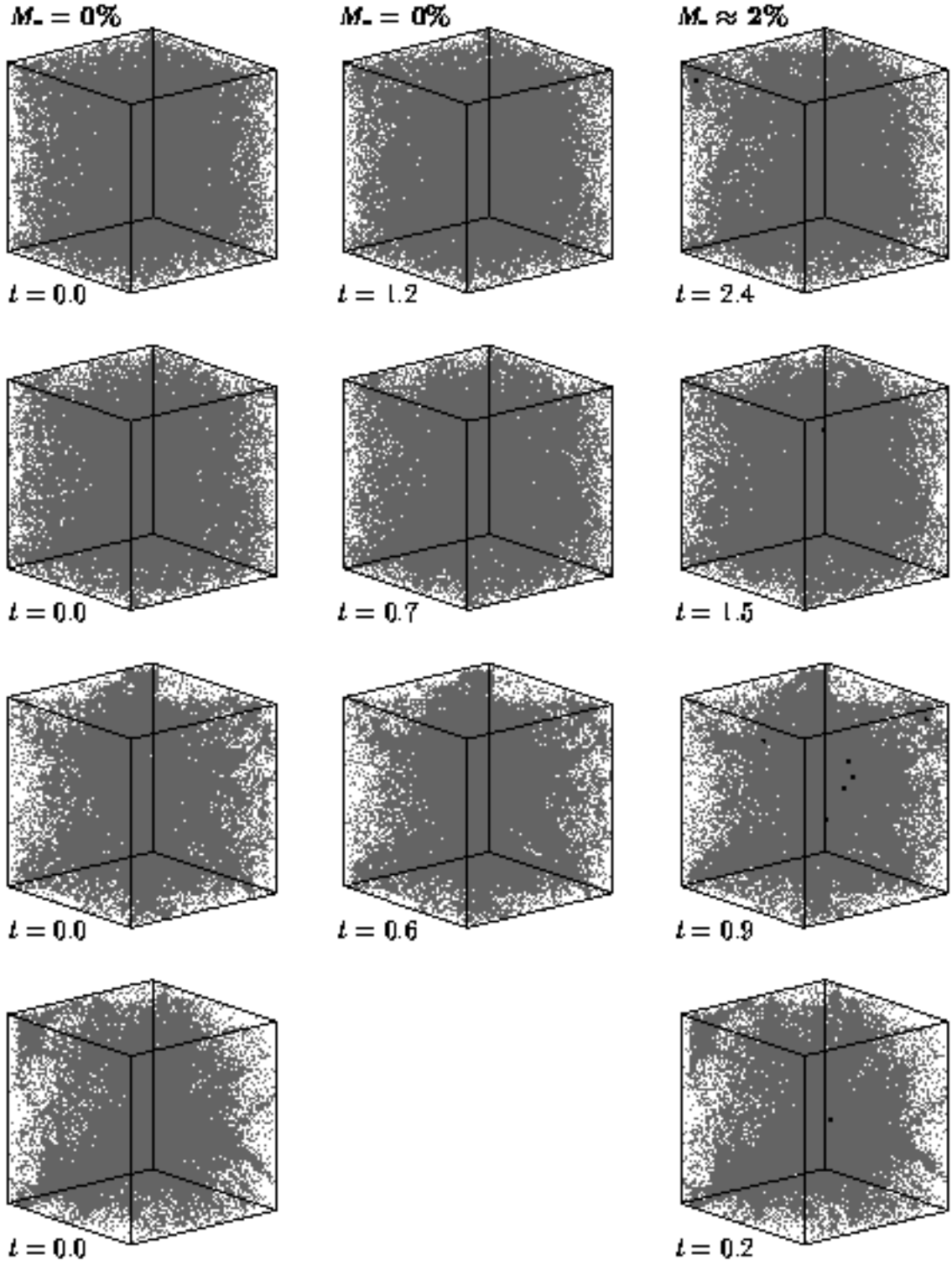


Fig. 1.— Comparison of the time evolution of four models with different initial power spectra $P(k) \propto 1/k^\nu$, initially (first column), after the first protostellar cores have formed (second column) and when $M_* \approx 2\%$ of the gas is converted into condensed cores. The first row plots model A0a with $\nu = 0$, the second row model A1a with $\nu = 1$, the third row model A2a with $\nu = 2$, the fourth row model A3a with $\nu = 3$.

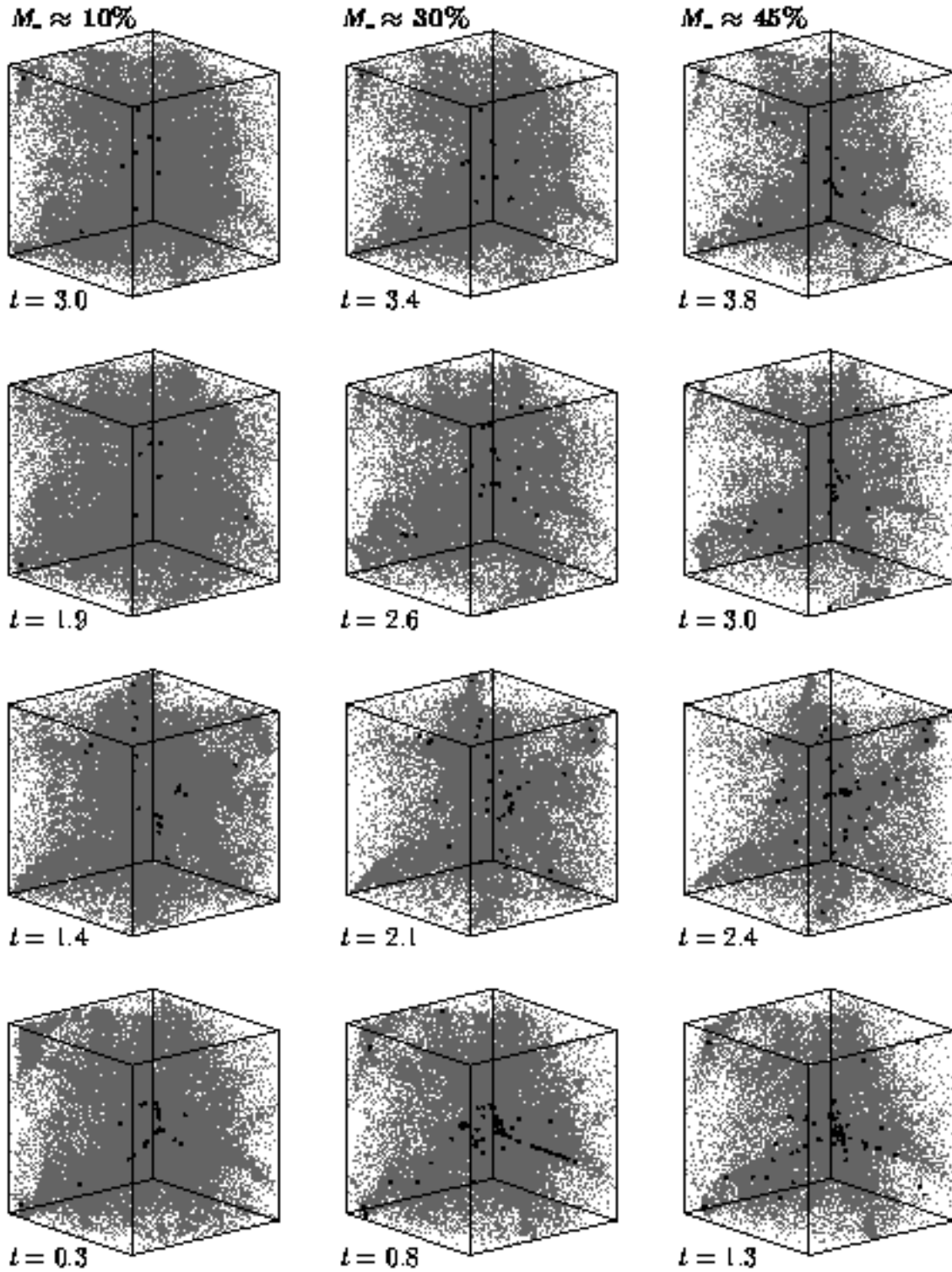


Fig. 1 — continued: Comparison of the time evolution of four models with different initial power spectra $P(k) \propto 1/k^\nu$: the distribution is plotted when $M_* \approx 10\%$ (first column), when $M_* \approx 30\%$ (center column) and when $M_* \approx 45\%$ of the available gas is accreted onto protostellar cores.

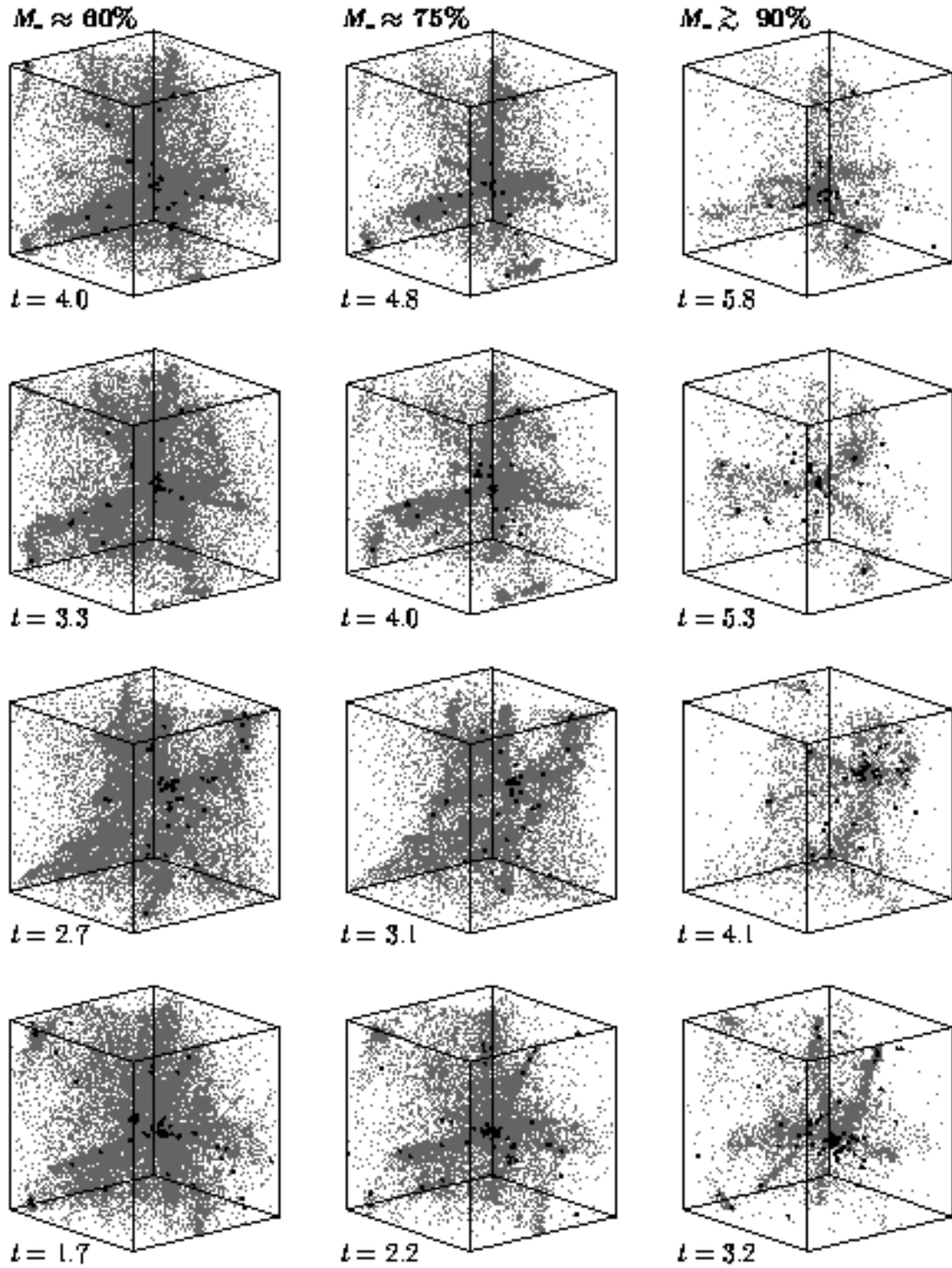


Fig. 1 — continued: Comparison of the time evolution of four models with different initial power spectra $P(k) \propto 1/k^N$: the distribution is plotted when $M_* \approx 60\%$ (first column), when $M_* \approx 75\%$ (center column) and when $M_* \gtrsim 90\%$ of the available gas is accreted onto protostellar cores.

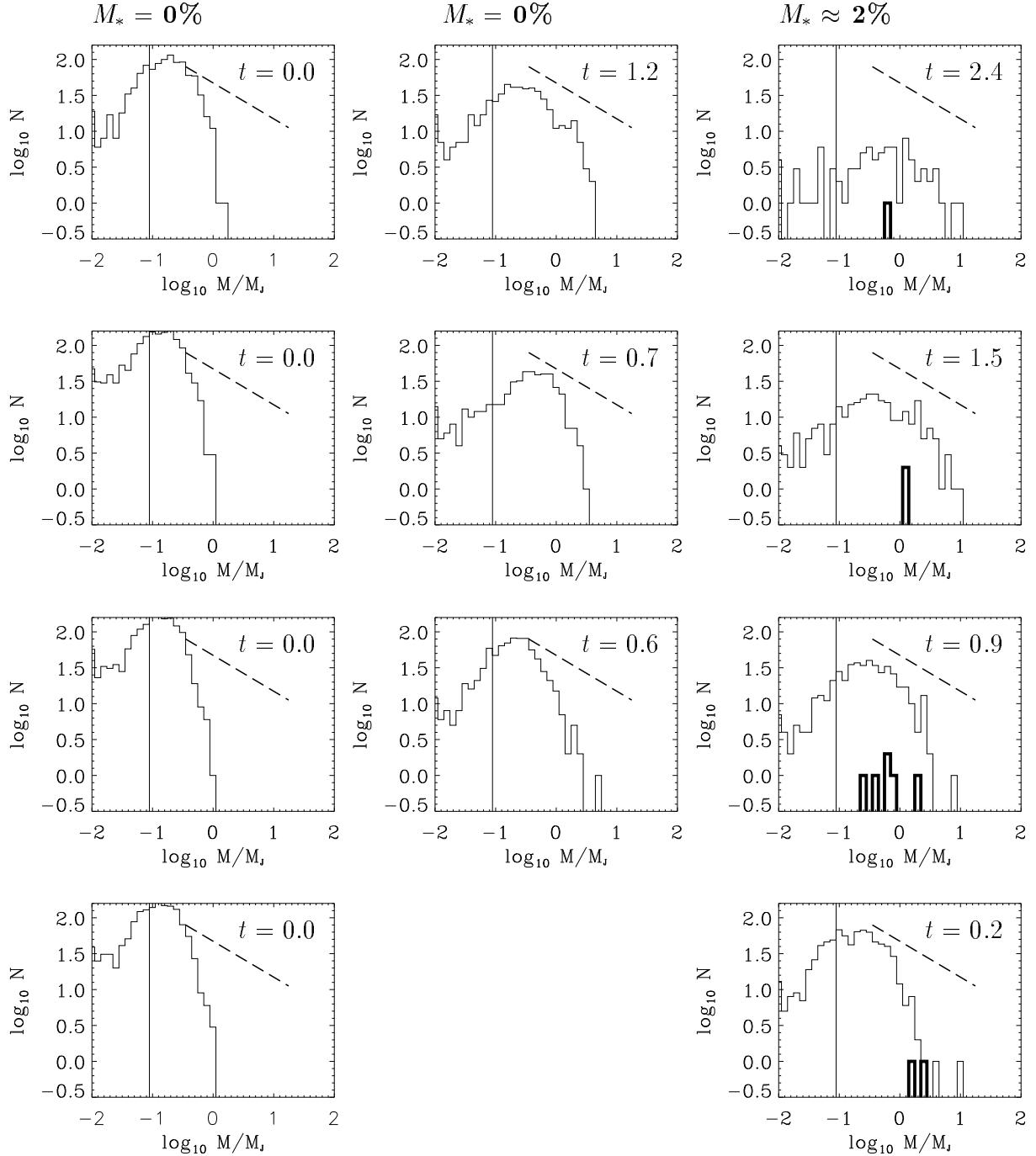


Fig. 2.— Mass spectrum of gaseous clumps (thin lines) and protostellar cores (thick) lines in models $\mathcal{A}0a$ (first row), $\mathcal{A}1a$ (second row), $\mathcal{A}2b$ (third row), and $\mathcal{A}3a$ (fourth row). Each column describes comparable evolutionary stages as defined by the fraction of mass converted into condensed cores M_* (analog to Fig. 1). The corresponding time is indicated separately in each plot. The thick dashed lines indicate the observed clump mass spectrum $dN/dm \propto m^{-1.5}$, whereas the horizontal lines give the resolution limit for the clump masses.

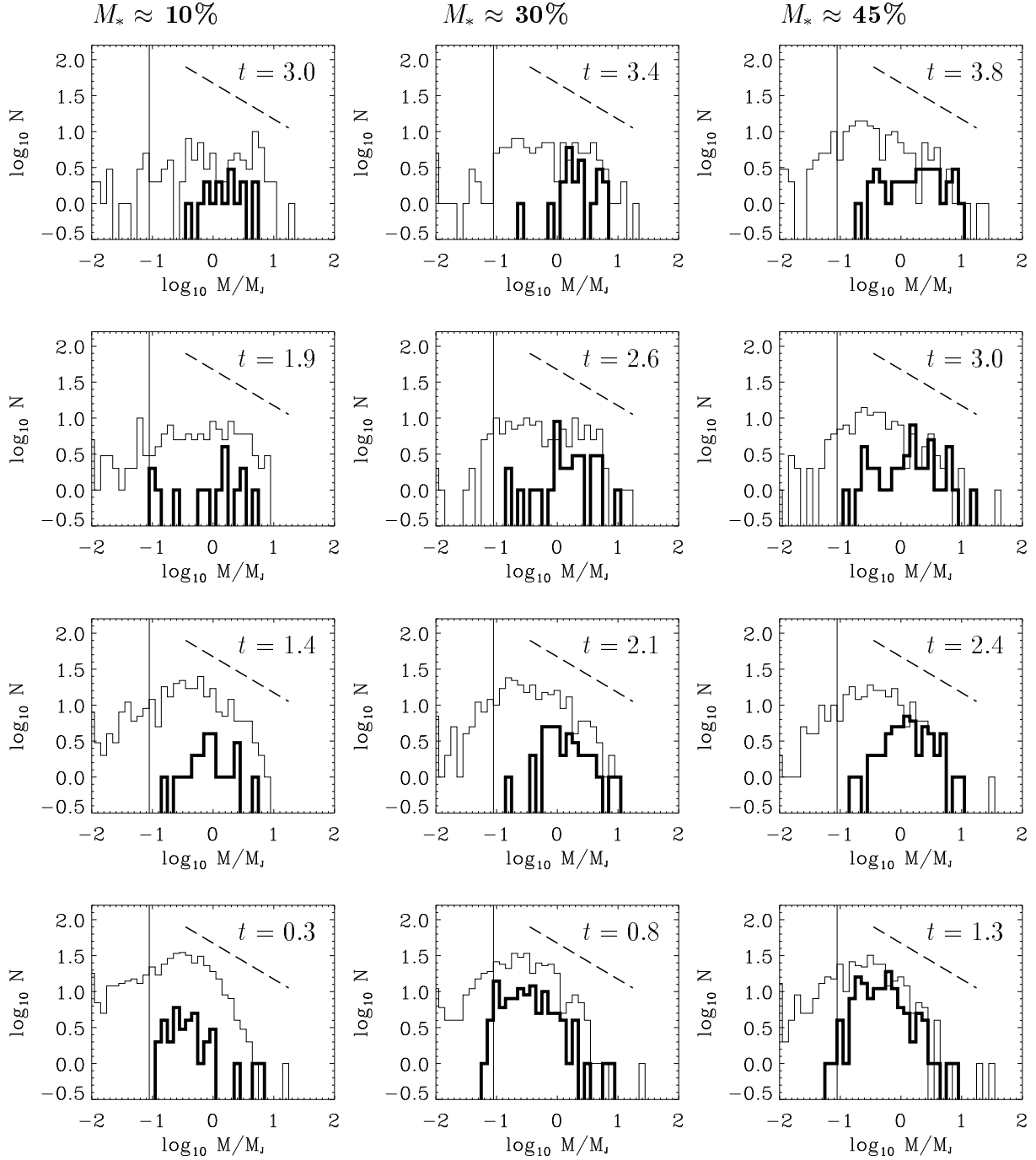


Fig. 2 — continued: Mass spectrum of gaseous clumps (thin lines) and protostellar cores (thick) lines in models $\mathcal{A}0a$ (first row), $\mathcal{A}1a$ (second row), $\mathcal{A}2b$ (third row), and $\mathcal{A}3a$ (fourth row) at phases of the evolution when $M_* \approx 10\%$, $M_* \approx 30\%$, and $M_* \approx 45\%$.

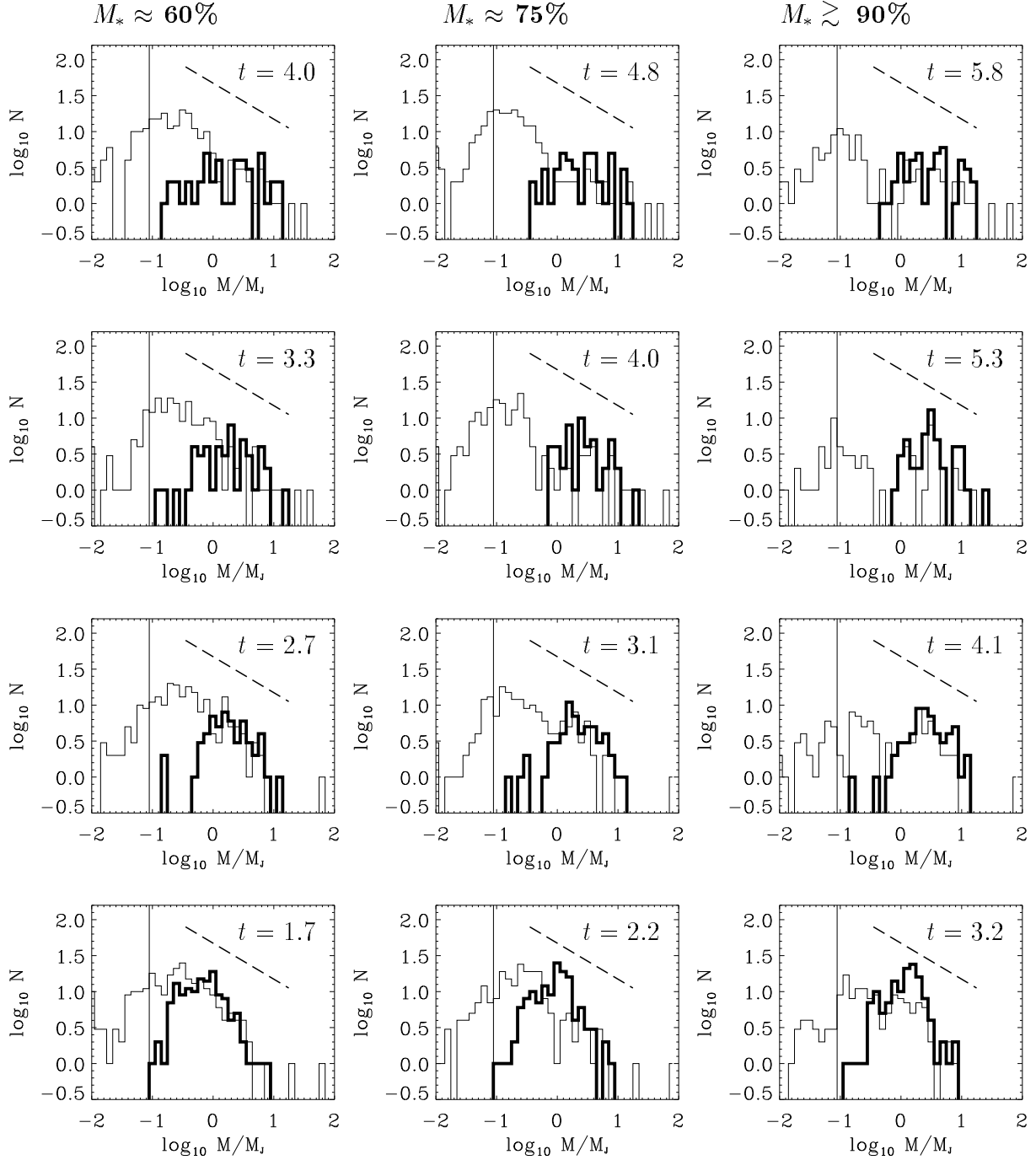


Fig. 2 — continued: Mass spectrum of gaseous clumps (thin lines) and protostellar cores (thick) lines in models $A0a$ (first row), $A1a$ (second row), $A2b$ (third row), and $A3a$ (fourth row) at evolutionary phases when $M_* \approx 60\%$, $M_* \approx 75\%$, and $M_* \geq 90\%$.

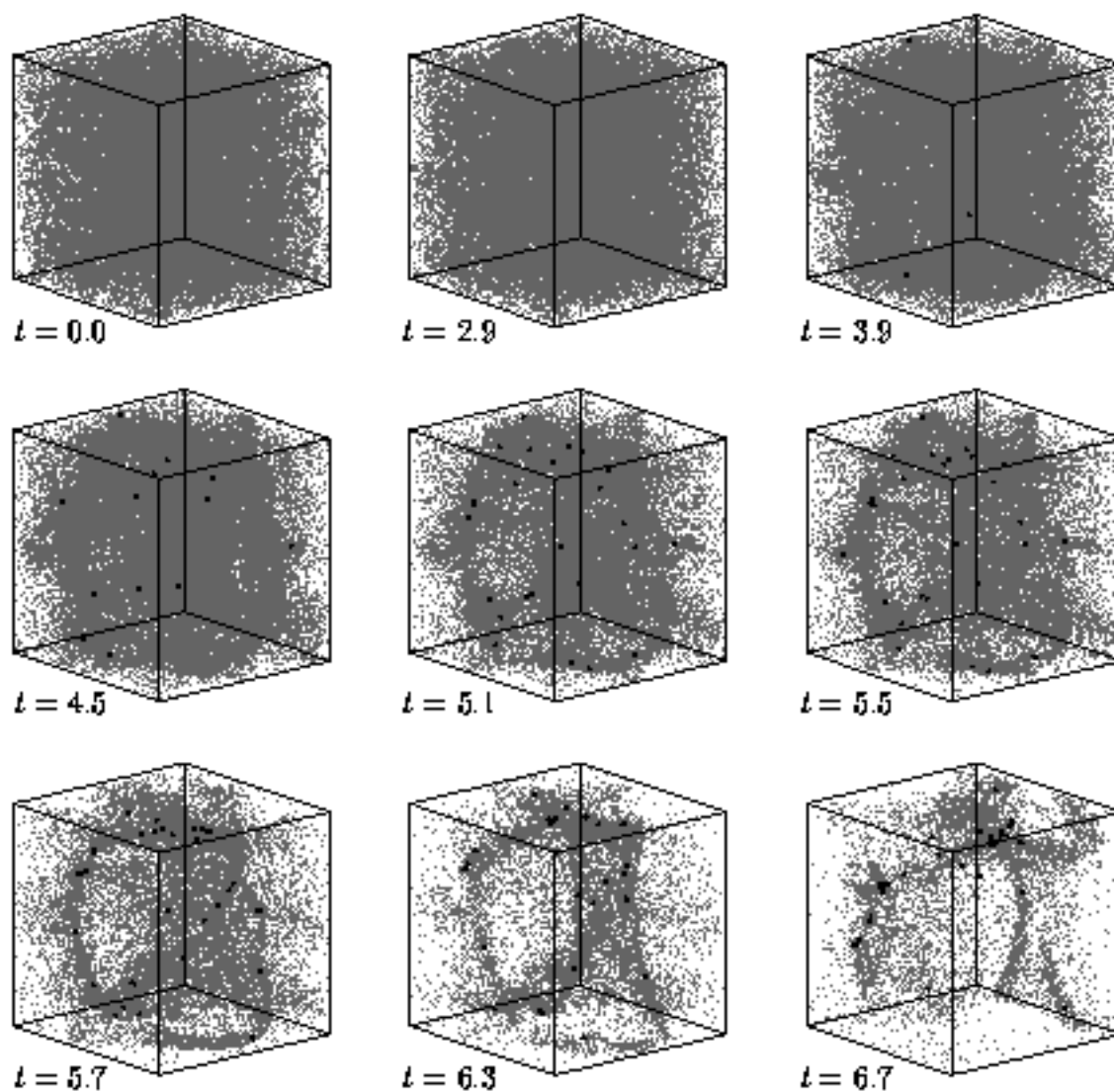


Fig. 3.— Time evolution of model *A1b*. It contains 5×10^5 SPH particles and the initial density distribution is generated from a fluctuation spectrum with $\nu = 1$ that is truncated for modes $k < 4$. The snapshots correspond to the following stages of the dynamical evolution: $t = 0.0$ – initial particle distribution, $t = 2.9$ – the maximum density contrast has reached half the value required to identify compact objects as protostellar cores, $t = 3.9$ – the first protostellar cores have formed and contain altogether $M_* = 2\%$ of the total gas mass, $t = 4.5$ – $M_* = 10\%$, $t = 5.1$ – $M_* = 30\%$, $t = 5.5$ – $M_* = 50\%$, $t = 5.7$ – $M_* = 60\%$, $t = 6.3$ – $M_* = 75\%$, and $t = 6.7$ – $M_* = 85\%$. For legibility, only every tenth non-accreted gas particle is displayed (small gray dots). Protostellar cores are denoted by large dark dots.

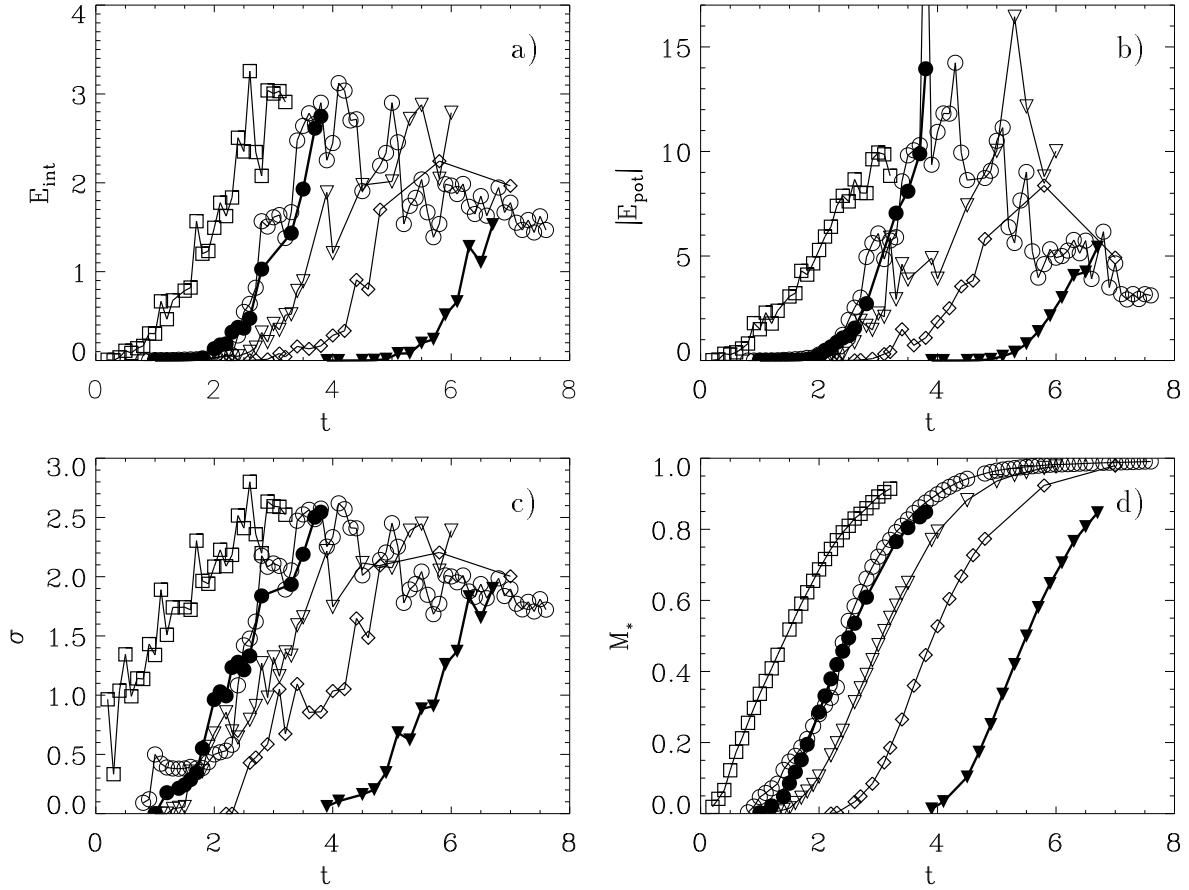


Fig. 4.— Time evolution of (a) the kinetic energy in random motions E_{int} , (b) the potential energy E_{pot} , (c) the velocity dispersion σ , and (d) the cumulative mass M_* in condensed cores for the clusters of protostellar cores that build up. The open diamonds denote model $\mathcal{A}0a$ with $\nu = 0$. There are two models with $\nu = 1$: $\mathcal{A}1a$ which is denoted by the open triangles and the high-resolution model $\mathcal{A}1b$ which is plotted with filled triangles (its initial fluctuation spectrum is truncated and contains only modes with $k \geq 4$). The circles denote models with $\nu = 2$: $\mathcal{A}2a$ (open circles) and the high-resolution model $\mathcal{A}2b$ (closed circles). Finally, model $\mathcal{A}3a$ with the steepest spectrum, $\nu = 3$, is characterized by open squares.

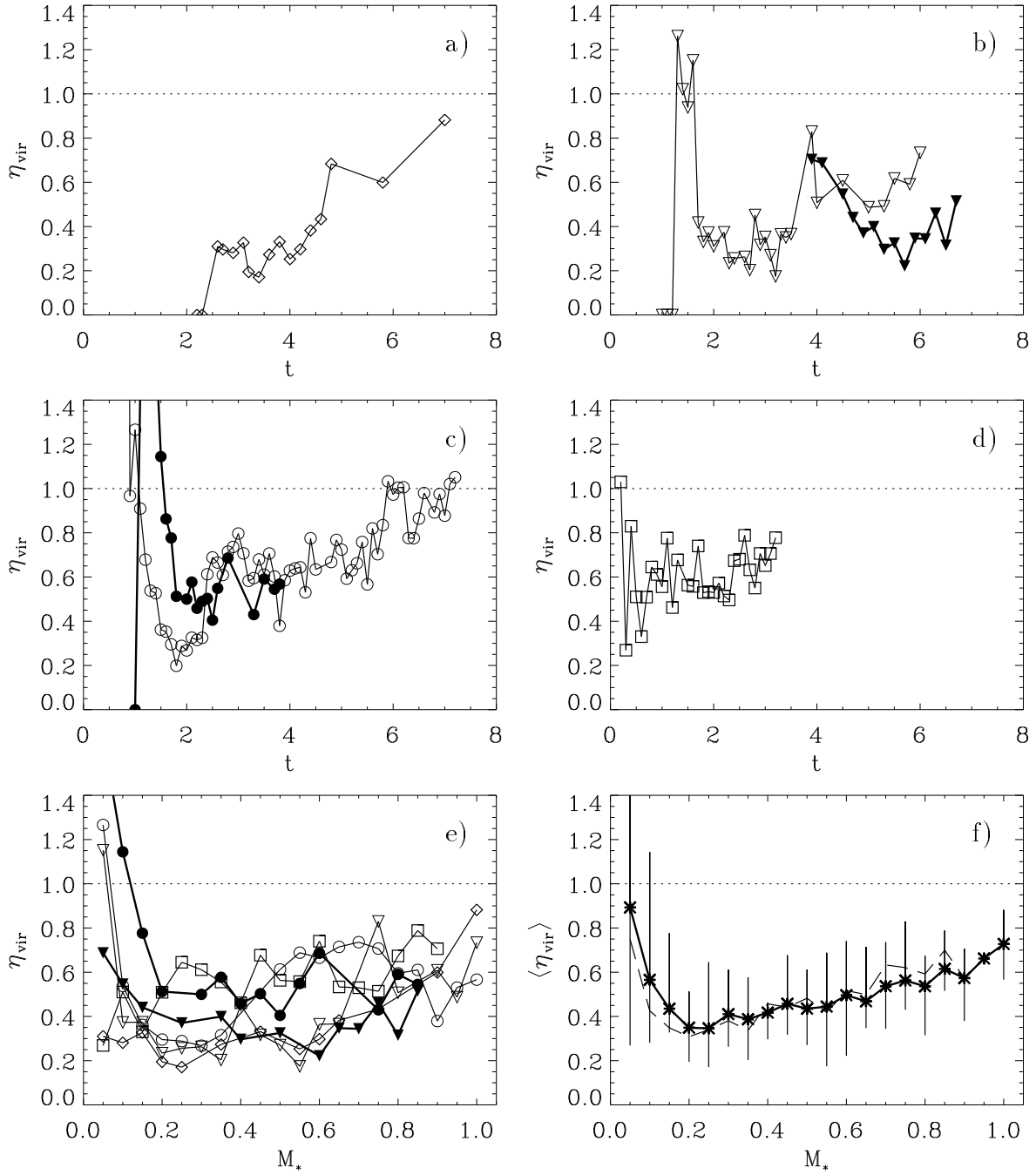


Fig. 5.— Time evolution of the virial coefficient η_{vir} : (a) for model $\mathcal{A}0a$, (b) for models $\mathcal{A}1a$ and $\mathcal{A}1b$, (c) for models $\mathcal{A}2a$ and $\mathcal{A}2b$, and (d) for model $\mathcal{A}3a$. The correspondence between each plotting symbol and model is analogous to Fig. 4. Plot of η_{vir} as function of the total mass fraction M_* accreted onto protostellar cores (e) for each model individually and (f) averaged over all models (thick solid line with error bars indicating the statistical deviations) and averaged over the four models with 2×10^5 particles (dashed line).

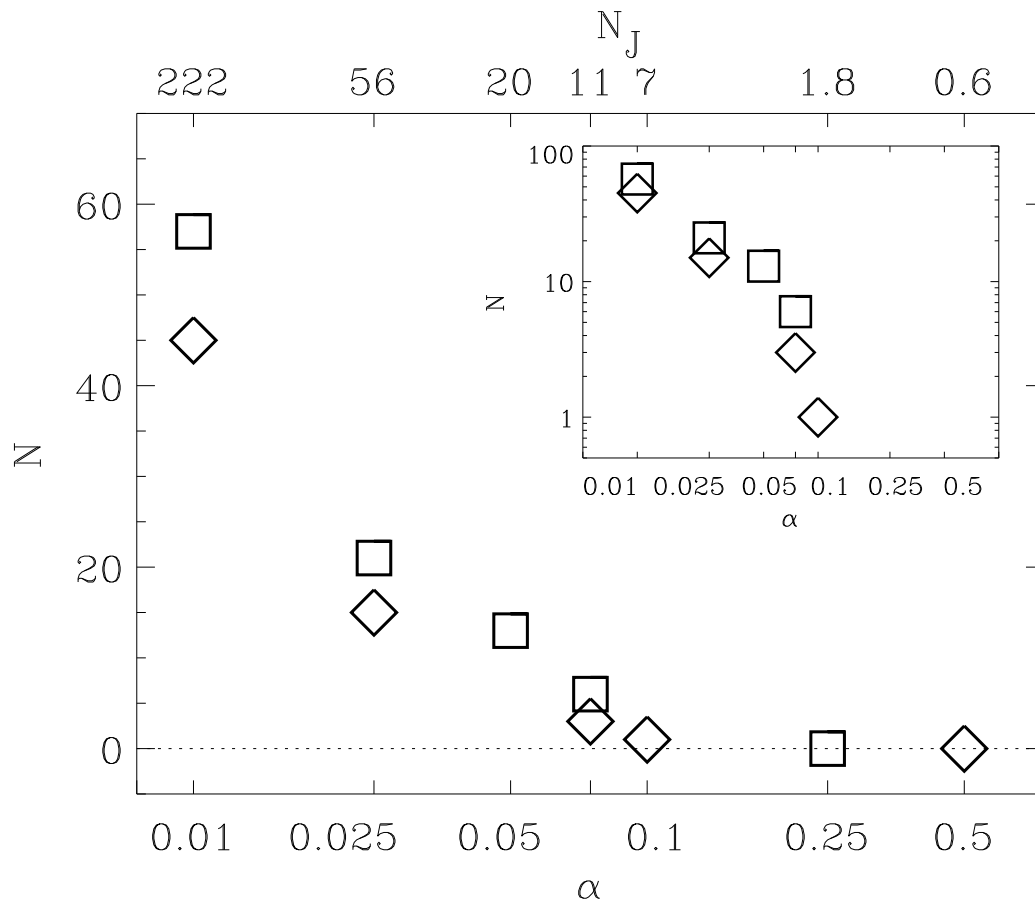


Fig. 6.— Total number N_* of protostellar cores that form during the dynamical evolution of the isothermal models listed in Tab. 2 as function of the temperature parameter α . Open diamonds denote the set of models with $\nu = 1$ and open squares denote models with $\nu = 2$; dimensionless temperatures are given on a logarithmic scale. The upper axis indicates the corresponding number of Jeans masses N_J contained in the considered volume. The inlay gives N_* scaled logarithmically to indicate that the number of protostellar cores declines with increasing temperature α roughly proportional to $\alpha^{-3/2}$.